Open Access Library Journal
2024, Volume 11, e12070
ISSN Online: 2333-9721
ISSN Print: 2333-9705

Development of a Portable Radioactive Aerosol Measuring Instrument Prototype

Mingjiang Wu, Min Gu*, Qinghai Wu, Dingding Xian

College of Nuclear Technology and Automation Engineering, Chengdu University of Technology, Chengdu, China
Email: *1355359701@qq.com

How to cite this paper: Wu, M.J., Gu, M., Wu, Q.H. and Xian, D.D. (2024) Development of a Portable Radioactive Aerosol Measuring Instrument Prototype. *Open Access Library Journal*, **11**: e12070.
https://doi.org/10.4236/oalib.1112070

Received: August 5, 2024
Accepted: September 23, 2024
Published: September 26, 2024

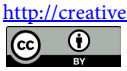

Abstract

At present, the portable radioactive aerosol measuring instrument prototype mainly adopts the cumulative measurement method, which requires personnel to regularly replace the filter, which is not conducive to online long-term measurement. Therefore, this paper designs a portable radioactive aerosol measuring instrument prototype that is easy to carry, high-precision, low-power, and small in size. Firstly, the internal and external structures were miniaturized. Secondly, low-power design was adopted for the hardware. Finally, based on the characteristics of radioactive aerosol particles, algorithm design and software design were carried out. The stability, airtightness, paper feeding accuracy, signal quality, and multi-channel performance of the instrument were verified through testing. The final result shows that the instrument can operate stably and continuously.

Subject Areas

Nuclear Chemistry

Keywords

Radon Detector, Hardware Design, Numerical Calculation, Paper Feed

1. Introduction

Radioactive aerosols pose great harm to humans, especially when inhaled, causing significant internal exposure. Accurate measurement of radioactive aerosol particle concentration is of great significance for accurately evaluating the hazards of radon exposure in the environment [1]. At present, the cumulative measurement method is basically used for radioactive aerosol measuring instruments in China, which requires personnel to regularly replace the filter, which is not conducive to online long-term measurement [2]. This article aims to develop a portable, high-precision, low-power, and small volume radioactive aerosol continuous monitoring

device. Used for continuous monitoring of radioactive aerosols, ensuring environmental safety and the physical health of nuclear related practitioners.

2. Overall System Design

The overall system diagram of the designed paper-based portable radon measurement device is shown in Figure 1. The portable radioactive aerosol measuring instrument prototype designed in this article consists of mechanical structure, signal acquisition circuit, micro multi-channel, main control circuit, hardware equipment, power system, human-computer interaction interface. The mechanical structure includes a measurement chamber and a hardware chamber. The measurement chamber is used for the signal acquisition and measurement of radioactive aerosols, while the hardware chamber houses the control board, lithium battery pack, and other hardware devices. The device is powered by a 12 V lithium battery, and a battery protection circuit and battery level monitoring circuit are designed. The battery voltage is converted to the required voltage for other chips and hardware devices using DC-DC, LDO, and charge pump chips. The micro multi-channel analyzer is used to acquire the spectrum of radon progeny. It is compact in size (20 mm × 42 mm) and has low power consumption (approximately 100 mW). A serial port screen is used as the human-machine interface, providing measurement interface, historical data viewing interface, and testing and debugging interface. The core chip of the control circuit is STM32F407ZET6. A FAT file system and an RT_thread real-time system are used for control, data acquisition from various sensors, acquiring multi-channel spectrum data in different measurement modes, and finally, spectral analysis and concentration calculation [3].

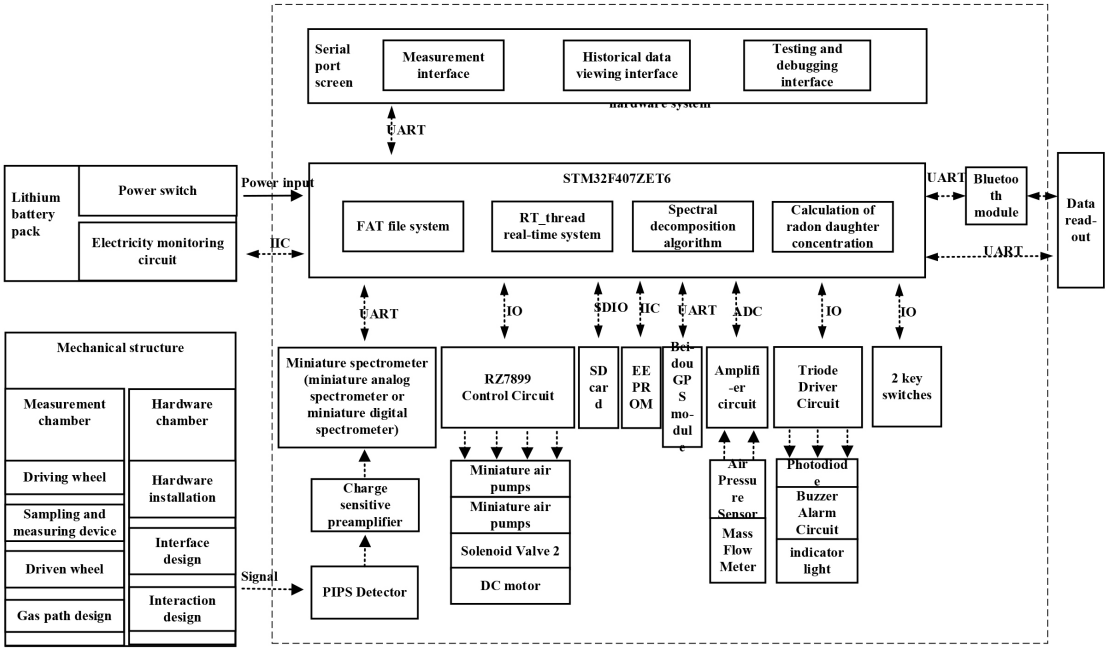

Figure 1. Block diagram of the overall system of the instrument.

3. Miniature Structure Design

1) Measurement Chamber Design

The measurement chamber is the core of the entire device and is used for sampling and measurement of radioactive aerosols. The design of the measurement chamber is based on the measurement method and mode of radon progeny. The measurement chamber is miniaturized based on the measurement method, including the main and driven wheels, sampling measurement device, paper feeding device, measurement device, gas path, and external interfaces [4]. The measurement chamber mainly consists of active wheels, driven wheels, DC motor, detection device (detector, charge sensitive preamplifier), solenoid valve, pressure sensor, filter paper, encoder composed of photodiodes, and aviation connectors. The measurement chamber needs to maintain a certain degree of airtightness. Rubber rings are used as sealing materials for the casing, and communication between the measurement chamber and the hardware chamber is established via aviation connectors. Figure 2 shows the mechanical structure of the measurement chamber of the portable continuous radon monitoring device.

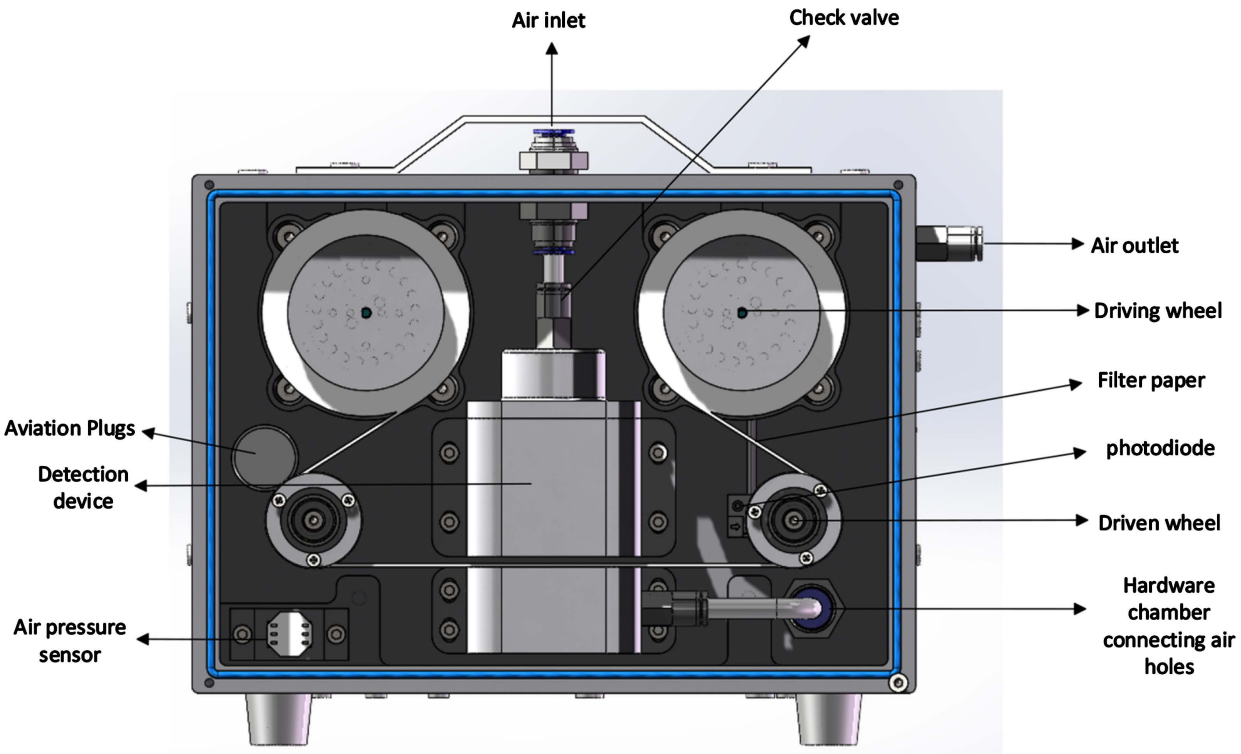

Figure 2. Measuring the mechanical structure of the chamber.

2) Sampling Chamber Design

The sampling and measuring device inside the measurement chamber is one of the core components of the continuous monitoring instrument, used for sampling radioactive aerosol particles and measuring signals of the continuous monitoring instrument [5]. The sampling measurement device consists of a detector and a

charge-sensitive preamplifier, which are used to acquire the signals of radioactive aerosol particles，As shown in Figure 3(a). The distance between the detector and the bottom filter paper in the sampling measurement device is approximately 5 mm. The upper port of the sampling measurement device is designed in a tapered shape As shown in Figure 3(b), and the internal structure is inclined [6], As shown in Figure 3(c). The internal surfaces are polished to improve the deposition of radon progeny particles on the surface of the filter paper, enhancing the detection efficiency of the device and facilitating the flow of radioactive particles. These designs greatly reduce tailing phenomena, improve particle detection efficiency, and lower the detection limit. As shown in Figure 3 for the instrument sampling measurement device design.

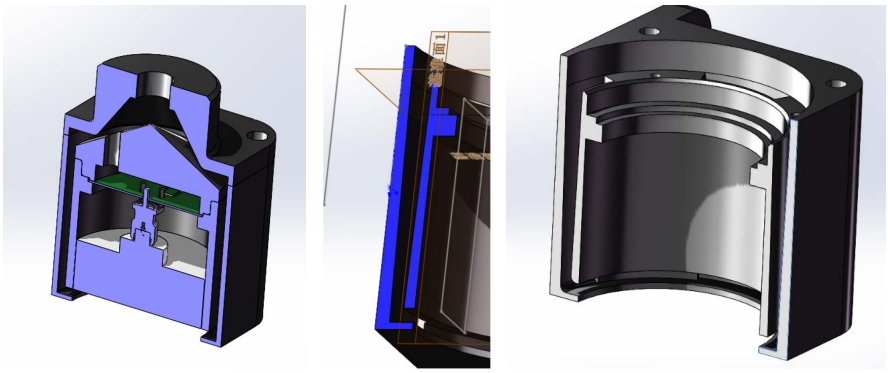

(a) (b) (c)

Figure 3. Instrument measuring device.

3) Paper walking structure design

In order to realize the continuous monitoring instrument continuous measurement function, continuous monitoring instrument design paper walking device and paper walking length measurement device. Paper walking device using micro DC motor and master-slave wheel combination design; paper walking length device using photodiode and slave wheel design. Instrument paper walking using control micro DC rotation for paper walking, where the design of the master wheel and slave wheel to guide the paper walking. In order to calculate the length of the walking paper, specifically designed to follow the structure of the wheel, 36 teeth in its head design, when the teeth through the photoelectric encoder will produce pulses, and then counted through the microcontroller counter, you can calculate the length of a single walk through the program and the total length of the walking paper. As Figure 4 for the instrument's paper walking device.

4. Instrument Hardware Circuit Design

The hardware system of this portable continuous monitor for radioactive aerosols can be divided into four parts: detector signal acquisition part, miniature multichannel part, power supply system design, main control circuit design part. Figure 5 shows the block diagram of the hardware structure of the instrument. In

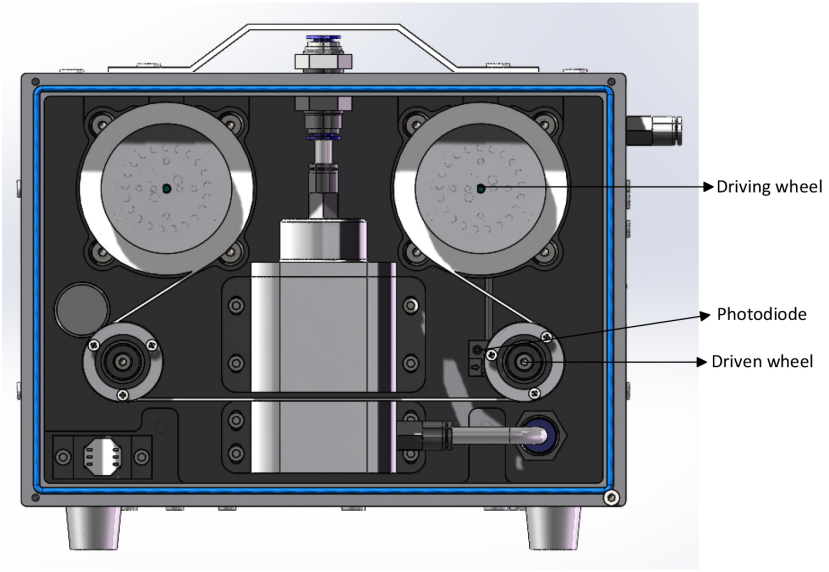

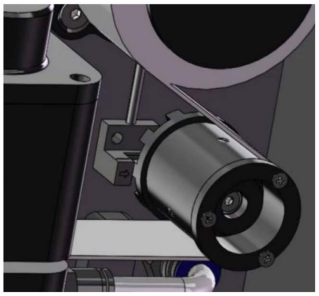

Figure 4. Paper conveyor and paper length measuring device.

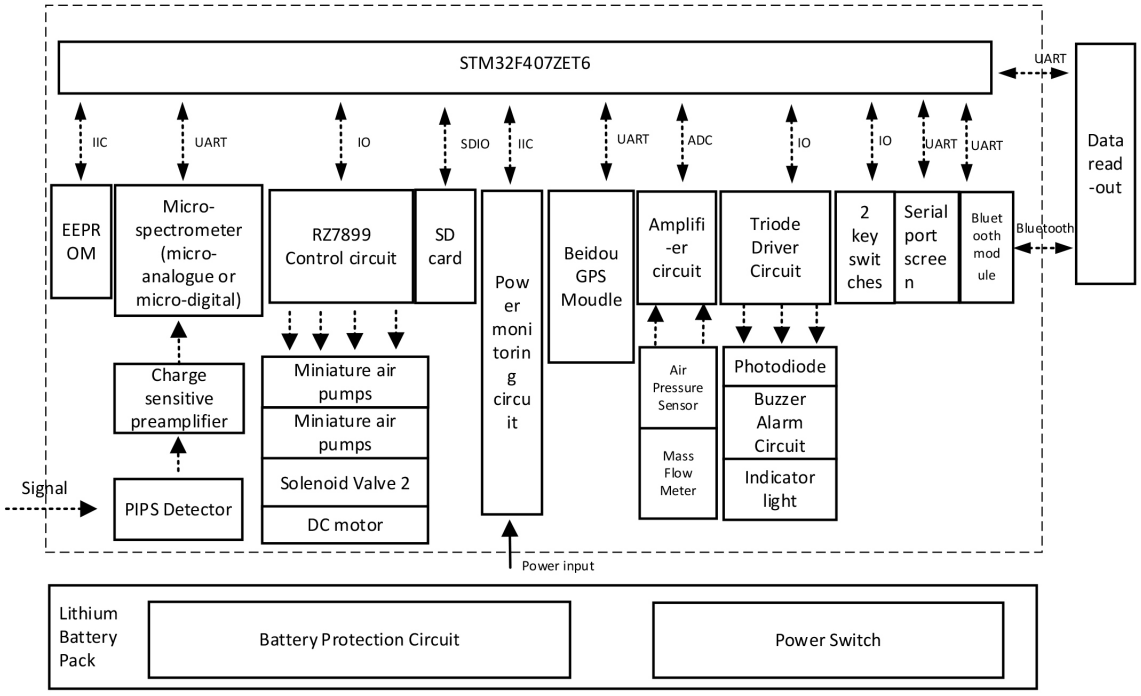

Figure 5. Block diagram of instrument hardware structure.

this paper, the hardware structure of the continuous monitoring instrument selects the passivated ion implantation silicon semiconductor detector and charge sensitive amplifier as the front-end signal readout circuit. And this instrument is designed with a miniature digital multi-channel for spectral operation of the front-end signal, which is characterized by small size and low power consumption. The miniature digital multi-channel is designed with a low-power chip STM32L432KBU6, LATTICE's FPGA ICE40UP5K, a high-speed ADC and a programmable amplifier. The main control circuit uses the STM32F407ZET6 chip as the core, and the control circuit is designed to control the rotation of the micro DC motor, the pumping of the air pump and the switching of the solenoid valve; the buzzer alarm circuit and the indicator light warning circuit are designed; the mass flow meter and barometer data acquisition circuit are designed; the timer is used to obtain the length of the paper walk; the serial port is used to obtain the location information of the BeiDou GPS module, the battery level The mass flow meter data acquisition circuit is designed; the timer is used to obtain the travel length; the serial port is used to obtain the position information of BeiDou GPS module, battery level, and spectral line data of the spectrometer; and the EEPROM and SD card are used as data storage units. Instrument and external communication interface through the serial port and Bluetooth module [7].

The micro digital multichannel programmable gain amplifier circuit is a combination of DAC and op amp, which is the same as the micro analog multichannel programmable amplifier. The single-ended differential chip used here is THS4561, which has extremely low power consumption. The input signal is converted into a differential signal and sent to the ADC chip. As **Figure 6** shows the block diagram of the miniature digital multi-channel system.

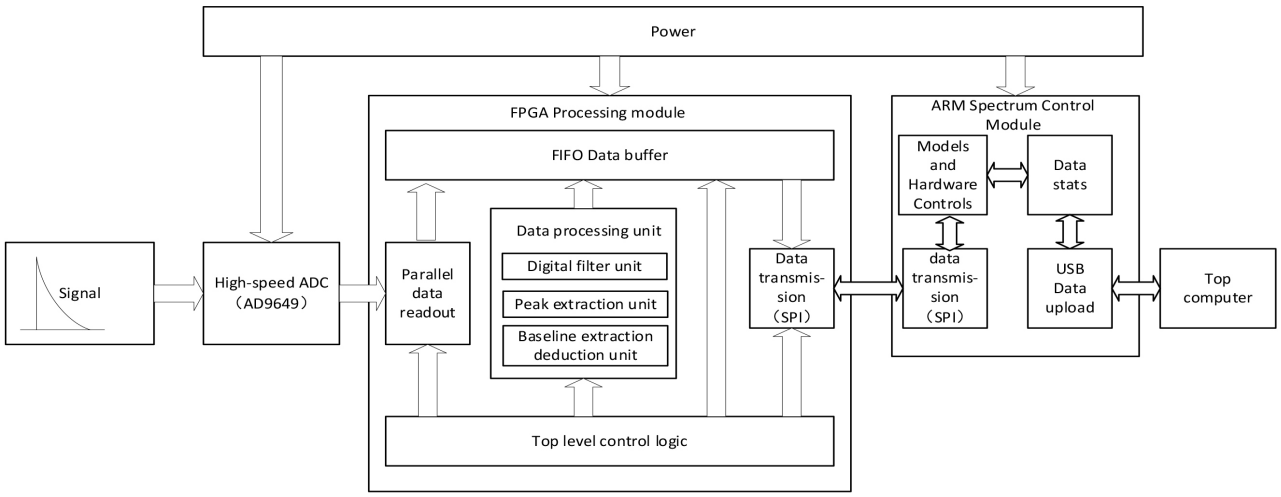

Figure 6. Block diagram of miniature digital multichannel system.

5. Radon Daughter Measurement Algorithm

1) Energy Zone Division

The energy zone of 6.00 Mev of ^{218}Po is 3.00 Mev - 6.20 Mev, which is the energy

zone 1;

The energy zone of 7.69 Mev of ^{214}Po is 6.20 Mev - 7.90 Mev, which is the energy zone 2;

The energy zone of 8.78 Mev of ^{212}Po is 7.90 Mev - 10 Mev, which is the energy zone 3;

2) Channel Addressing of Energy Zones Converting Energy Zones 1, 2, 3 into Channel Addresses

Step 1: During the test phase, firstly, the original peak positions of ^{218}Po and ^{214}Po are found manually by taking long time samples and measurements. Corresponding to E_1 = 6.0 Me V Road address is ch_1; E_2 = 7.69 Me V Road address is ch_2;

Step 2: Solve the equations to find the values;

$$a = \frac{ch_1 - ch_2}{E_1 - E_2} \tag{1}$$

$$b = ch_1 - \frac{ch_1 - ch_2}{E_1 - E_2} \cdot E_1 \tag{2}$$

Step 3: Convert the energy to road address Utilize the following equations:

$$ch = aE_\alpha + b \tag{3}$$

Here, denotes the particle energy in Me V; *Ch* denotes the corresponding channel number.

The energy intervals of energy region 1, energy region 2, and energy region 3 are converted into channel address intervals.

3) Concentration and Potential Calculation

Step 1: Sample for 15 minutes at a sampling flow rate of 3 L/min, then stop sampling and begin measurement for 105 minutes.

Step 2: Record the cumulative spectra at the 12th, 30th, 43rd, and 105th minutes of sampling. The cumulative spectrum at the 12th minute is designated as Spectrum A, the difference between the cumulative spectra at the 30th and 12th minutes is designated as Spectrum B, the cumulative spectrum at the 43rd minute is Spectrum C, and the difference between the cumulative spectra at the 105th and 43rd minutes is Spectrum D.

Step 3: On spectral line A, compute the sum of the counts on energy region 1, denoted N11.

On spectral line A, compute the sum of the counts on energy region 2, denoted N21.

On spectral line B, calculate the sum of the counts on energy region 2, denoted N22.

On spectral line C, calculate the sum of the counts on energy region 3, denoted N31.

On spectral line D, calculate the sum of the counts on energy region 3, denoted N32.

Step 4: Calculate coefficients.

$$H = \frac{1}{vE\eta K} \tag{4}$$

V sampling flow rate, 3 L/min, E detection efficiency 0.1987 (or measured), membrane filtration efficiency, 0.987, K membrane self-absorption coefficient 0.978.

Step 5: Calculate the concentration of each sub-body.

Calculation: Concentrations of RaA (^{218}Po), RaB (^{214}Pb), RaC (^{214}Bi), ThB (^{212}Pb), and ThC (^{212}Bi)

Concentration of ^{218}Po

$$C_{po218} = C_2^1 = 1.5638 \times H \times N_{11} \tag{5}$$

Concentration of ^{214}Pb

$$C_{pb214} = C_3^1 = H \times \left(-0.1941 \times N_{11} - 0.3182 \times N_{21} + 0.286 \times N_{22}\right) \tag{6}$$

Concentration of ^{214}Bi

$$C_{Bi214} = C_4^1 = H \times \left(0.0291 \times N_{11} + 0.3453 \times N_{21} - 0.1468 \times N_{22}\right) \tag{7}$$

Concentration of ^{212}Pb

$$C_{pb212} = C_5^1 = H \times \left(-0.0316 \times N_{31} + 0.0323 \times N_{32}\right) \tag{8}$$

Concentration of ^{21}2Bi

$$C_{Bi212} = C_6^1 = H \times \left(0.05 \times N_{31} - 0.0125 \times N_{32}\right) \tag{9}$$

Step 6: Calculate the potential.

The total energy emitted by the α particles when all the sub-bodies of radon decay to ^{210}Pb is called the "radon sub-body α potential," with the unit J·m^{-3}.

$$PAEC_{Rn} = 0.000579C_{po218} + 0.00285C_{pb214} + 0.002087C_{Bi214} \tag{10}$$

The sub-body α potential of thorium is measured in J·m^{-3}.

$$PAEC_{Th} = 0.07097C_{pb212} + 0.006735C_{Bi212} \tag{11}$$

Once the calculation is complete, the data is displayed, the paper is advanced, and the next cycle begins with Step 1.

6. Software Design

The design of the instrument program can be divided into several parts: the main control board program, the micro-digital multi-channel program, and the serial port screen interaction design. The main control board program is the core program of the instrument, connecting all hardware devices [8]. It controls, communicates, and processes data for all devices based on the measurement method, measurement mode, human-machine interaction, and hardware device characteristics. The overall modular framework of the instrument programis shown in **Figure 7**.

The main control board program uses the domestic RT_thread real-time operating system and FAT file system as the foundation, and utilizes a multi-threaded and modular approach to program design. The main control board program can

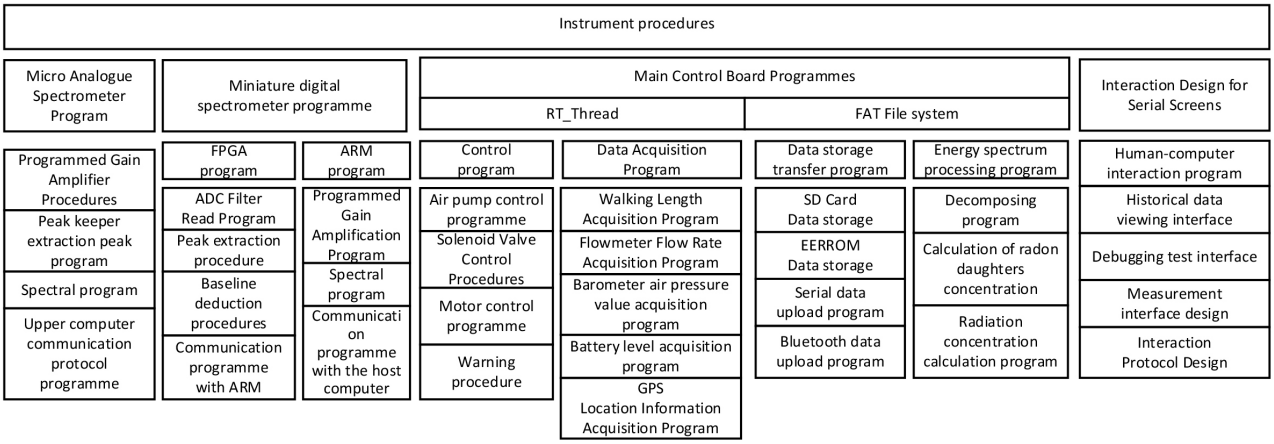

Figure 7. Modular block diagram of instrument program.

be divided into five parts: instrument hardware device control program, hardware device data acquisition program, data storage and transmission program, spectrum processing program, and serial port screen interaction program. The instrument hardware device control program includes the pump control program, solenoid valve control program, motor control program, and alarm program. The hardware device data acquisition program includes the paper length acquisition program, mass flowmeter flow rate acquisition program, barometric pressure acquisition program, battery level acquisition program, and GPS location information acquisition. The data storage and transmission program includes the SD card data storage program, EEPROM data storage program, serial port external data transmission program, and Bluetooth external data transmission program. The spectrum processing program includes the spectrum analysis program and concentration calculation program [9]. The serial port interaction program mainly controls the main control board to perform corresponding hardware operations by sending and processing commands through the serial port screen.

7. Testing

1) Paper Advancement Error Testing

In continuous measurement mode, the instrument automatically advances the paper. The paper advancement error needs to be controlled within a certain range to ensure the paper is advanced accurately, to calculate the remaining paper length, and to enable continuous measurement. Otherwise, the instrument may not advance the paper accurately when working in continuous measurement mode, leading to situations such as running out of filter paper, excessive remaining paper, or waste. Table 1 shows the instrument's paper advancement error table, with the paper advancement distance, the actual paper advancement length, and the error value calculated by taking the absolute value of the difference between the actual paper advancement length and the paper advancement distance. The method of testing involves setting the paper advancement length via the interface, and then measuring the paper advancement length with a flow standard

caliper when the paper stops advancing. The final result shows that the paper advancement error of the instrument is approximately 0.5 mm each time. Assuming a paper length of 10 m, with the paper advancing by 10 cm each time, a total of 100 measurements can be made with an error of 5 cm, resulting in a paper waste rate of 0.5%, meeting the requirements [10].

Table 1. Paper error test.

Group	Paper travel distance	Actual paper walking	Error value
1	31.4 mm	31.9 mm	0.5 mm
2	62.8 mm	63.4 mm	0.6 mm
3	94.2 mm	94.6 mm	0.4 mm
4	31.4 mm	31.8 mm	0.4 mm
5	31.4 mm	32 mm	0.6 mm

2) Stability Testing

After the system undergoes mechanical processing and installation, several hardware device tests were conducted to ensure the normal operation of control devices, the sensor data collection deviation of less than 1%, and the leak-tightness during measurements. Subsequently, the instrument was tested for continuous measurement mode, with 18 measurements set up, each lasting a half hour for both sample collection and measurement [11]. The test results showed that the automatic control process of the system was error-free, all devices did not overheat, and the system software did not crash or freeze, thus meeting the requirements for integrity and stability of online monitoring. The physical diagram of the system's operation testing is shown in Figure 8.

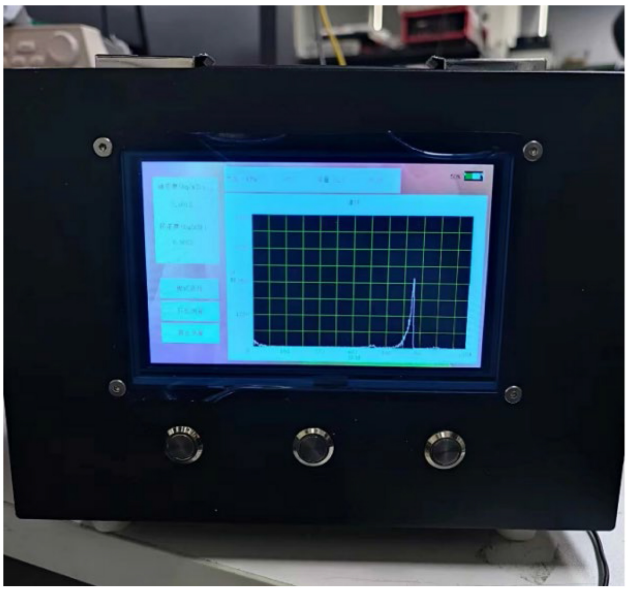

Figure 8. Physical diagram of system operation test.

a) Peak Drift Testing

During the process of measuring multiple spectra of radioactive aerosols, changes in parameters of electronic components due to factors such as temperature and electron drift may cause shifts in the peak positions of the measured spectra. The drift of the peak positions can determine the stability of the instrument, which also affects the subsequent spectrum processing [12]. Therefore, it is necessary to test the peak drift performance of the system. The test involves continuous air sampling, recording and statistical analysis of the peak position of the ^{214}Po (7.68 MeV) characteristic peak of the radon sub-body. With a half-hour sample collection time and half-hour measurement time for 10 consecutive measurements, the test results, as shown in Table 2, indicate that the peak drift does not exceed ±1 channel. Thus, the stability of the system under this mode is relatively good and can meet the monitoring requirements.

Table 2. Peak drift test results of filtration membrane adsorption in single operation mode (total energy spectrum address: 1024 channels).

Measurement number	1	2	3	4	5	6	7	8	9	10
Peak position	768	767	768	768	768	767	769	768	768	767

b) Energy Resolution Testing

Energy resolution is an important indicator, characterizing the ability of the system to resolve nearby energy peaks [13]. A smaller energy resolution indicates better resolution capability. In natural environments, this study mainly extracted and analyzed the characteristic peak information of the radon sub-body ^{214}Po (7.68 MeV). The experimental test results, as shown in Table 3, indicate an average energy resolution of 1.341 from three measurements, with the actual energy resolution of the system being approximately 1.341% at 7.68 MeV.

Table 3. Actual energy resolution.

Measurement number	Actual energy resolution (%)
1	1.375
2	1.297
3	1.351

8. Conclusion

This article designs and develops a portable radioactive aerosol measuring instrument prototype. This study designed and developed a prototype of a portable radon sub-body measurement instrument using a paper advancement method. The instrument is composed of a mechanical structure, signal acquisition circuit, micro-multi-channel, main control circuit, hardware devices, power supply system, and human-machine interaction interface. After testing, the performance of the

prototype can basically meet the requirements. The next step will focus on further optimizing the process and improving its performance.

Fund Project

Sichuan Provincial Science and Technology Plan Project Task Book (Key R & D Projects 2023YFG0347) Research and application of online measurement technology for airborne radioactive aerosols.

Conflicts of Interest

The authors declare no conflicts of interest.

References

[1] Kadir, A.M., Zhang, L., Guo, Q.J., *et al.* (2014) Research on Accurate Measurement Method of Radon Daughters Concentration. *Radiation Protection*, **34**, 297-303.

[2] Liu, L.J., Xiao, D.T. and Lei, J.R. (2007) Development of a Continuous Radon Daughter Measurement Instrument. *Atomic Energy Science and Technology*, **41**, 509-512.

[3] World Health Organization (2017) Guidelines for Drinking-Water Quality: Fourth Edition Incorporating the First Addendum.

[4] Pan, L.T., Guo, Z.R., Huang, X.J., *et al.* (2023) Study on the Energy Spectrum of Radon Daughter Aerosol Adsorbed on Filter Paper. *Nuclear Electronics and Detection Technology*, **43**, 1090-1095.

[5] Marchais, T., Perot, B., Carasco, C., Ma, J., Allinei, P., Toubon, H., *et al.* (2020) Characterization of Uranium Ore Samples by HPGe Gamma-Ray Spectroscopy. *IEEE Transactions on Nuclear Science*, **67**, 654-661. https://doi.org/10.1109/tns.2020.2966824

[6] Wang, P., Pu, X., Wang, X.Q., *et al.* (2022) Design of a New Intelligent Radon and Radon Daughter Measurement Instrument. *Nuclear Electronics and Detection Technology*, **42**, 1101-1107.

[7] Yamamoto, S., Tarutani, K., Yamasoto, K., Iskandar, D. and Iida, T. (2001) Development of a Continuous Radon Concentration Monitoring System in Underground Soil. *IEEE Transactions on Nuclear Science*, **48**, 391-394. https://doi.org/10.1109/23.940086

[8] Khayat, O. and Afarideh, H. (2014) Heavy Charged Particle Nuclear Track Counting Statistics and Count Loss Estimation in High Density Track Images. *IEEE Transactions on Nuclear Science*, **61**, 2727-2734. https://doi.org/10.1109/tns.2014.2352174

[9] Roubal, Z., Szabó, Z., Kadlec, R. and Zdražil, L. (2023). Concentration and Mobility of Air Ions in the Environment of the Cisarska Cave (moravia). 2023 *Photonics & Electromagnetics Research Symposium*, Prague, 3-6 July 2023, 2193-2199. https://doi.org/10.1109/piers59004.2023.10221433

[10] Rabi, R., Oufni, L. and Badry, H. (2021). Measurements and CFD Modeling of Outdoor Radon Dispersion. 2021 7*th International Conference on Optimization and Applications*, Wolfenbüttel, 19-20 May 2021, 1-7. https://doi.org/10.1109/icoa51614.2021.9442664

[11] Tian, X.Y. (2023) Development of a Groundwater Radon Concentration Monitoring System Based on Gamma Spectroscopy. Master's Thesis, Donghua University of Technology.

[12] Zhang, J.X., Gu, Y., Wan, Q.Y., *et al.* (2021) Optimization Based on Energy Spectrum Tailing and Detection Efficiency Testing *α* Research on the Selection of Filter Membranes for Radioactive Aerosol Sampling. *Nuclear Technology*, **44**, 32-38.

[13] Li, Y. and Zhao, G.Z. (2020) Rain during the Song Dynasty Measurement of ~(222) Rn Daughter Detection Efficiency Using MC Simulated HPGe Detector. *Nuclear Electronics and Detection Technology*, **40**, 210-215.